European Polymer Journal 106 (2018) 214–222

Contents lists available at ScienceDirect

European Polymer Journal

journal homepage: www.elsevier.com/locate/europolj

Development and characterization of xyloglucan-poly(vinyl alcohol) hydrogel membrane for Wireless Smart wound dressings

Alessia Ajovalasit[a], Maria Cristina Caccami[b], Sara Amendola[c], Maria Antonietta Sabatino[a,*], Gioacchino Alotta[d], Massimiliano Zingales[d], Daniela Giacomazza[e], Cecilia Occhiuzzi[c], Gaetano Marrocco[b,c], Clelia Dispenza[a,e]

[a] Dipartimento dell'Innovazione Industriale e Digitale (DIID), Università degli Studi di Palermo, Viale delle Scienze Ed.6, 90128 Palermo, Italy
[b] Dipartimento di Ingegneria Civile ed Informatica, Università degli Studi di Roma Tor Vergata, Via del Politecnico 1, 00133 Rome, Italy
[c] RADIO6ENSE srl, Università degli Studi di Roma Tor Vergata, Via del Politecnico 1, 00133 Rome, Italy
[d] Dipartimento di Ingegneria Civile, Ambientale, Aerospaziale e dei Materiali, Università degli Studi di Palermo, Viale delle Scienze Ed. 8, 90128 Palermo, Italy
[e] Istituto di BioFisica (IBF), Consiglio Nazionale delle Ricerche, Via U. La Malfa, 153, 90146 Palermo, PA, Italy

ARTICLE INFO

Keywords:
Hydrogels
Wound dressings
Dielectric properties
Swelling
RFID sensors
Epidermal electronics

ABSTRACT

Hydrogel-based smart wound dressings that combine the traditional favourable properties of hydrogels as skin care materials with sensing functions of relevant biological parameters for the remote monitoring of wound healing are under development. In particular, lightweight, ultra-high frequency radiofrequency identification (UHF RFID) sensor are adjoined to xyloglucan-poly(vinyl alcohol) hydrogel films to battery-less monitor moisture level of the bandage in contact with the skin, as well as wireless transmit the measured data to an off-body reader. This study investigates the swelling behavior of the hydrogels in contact with simulated biological fluids, and the modification of their morphology, mechanical properties, and dielectric properties in a wide range of frequencies (10^0–10^6 Hz and 10^8–10^{11} Hz).

The films absorb simulated body fluids up to approximately four times their initial weight, without losing their integrity but undergoing significant microstructural changes. We observed relevant linear increases of electric conductivity and permittivity with the swelling degree, with an abrupt change of slope that is related to the network rearrangements occurring upon swelling.

1. Introduction

Chronic wounds and ulcers are particularly distressful for patients and challenging for health care providers and national health provisions [1].

Patients generally suffer for relentless pain, discomfort caused by malodour, need of frequent inspections and medication [2,3]. Moreover, chronic wounds are highly susceptible to infection. Choosing a proper dressing is a challenging aspect of wound care, because there is no single dressing that suits all wounds; indeed, the biochemical healing pattern is dependent on cells type, healing phase and can be complicated by comorbidity.

Protection from infection and traumas is the most fundamental and traditional role of wound dressings in the medical practice [3,4]. In more recent times, further features have been added, such as the ability to provide oxygenation, hydration, absorption of wound fluids and exudates, to release growth factors, to prevent and treat infectious states through the incorporation of anti-microbial agents [5,6].

Hydrogels are optimal candidates as wound dressing materials [7–9]. They are hydrophilic networks with the ability to retain a significant amount of water [10]. Therefore, they can absorb and retain exudates and necrotic tissue, together with the biological components, for example proteinases, that are deleterious for wound healing, while concurrently providing appropriate levels of hydration [11,12]. Indeed, an optimal level of hydration is required for the best wound management; excessive moisture results in maceration, while too little hydration results in wound drying and impaired tissue regrowth [13].

Hydrogel wound dressings are generally non-adhesive to the skin and high conformable, therefore particularly apt to be used in patients with thin or fragile skins [14]. Hydrogels can be self-standing films, coatings of textiles and non-woven mats, or adjoined with other synthetic materials.

The incorporation of diagnostic tools in wound dressings to measure biologically relevant parameters can be of great support for chronic

* Corresponding author.
E-mail address: mariaantonietta.sabatino@unipa.it (M.A. Sabatino).

https://doi.org/10.1016/j.eurpolymj.2018.07.038
Received 12 June 2018; Received in revised form 19 July 2018; Accepted 23 July 2018
Available online 24 July 2018

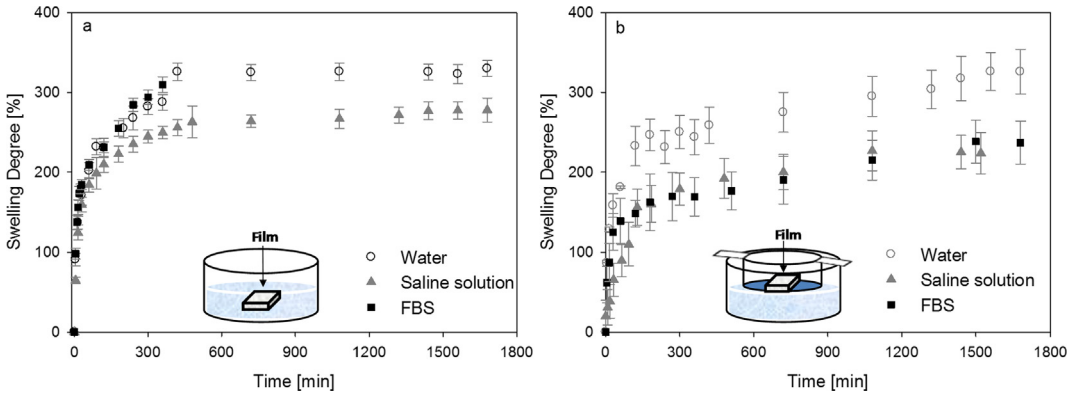

Fig. 1. Swelling behaviour of XG-PVA immersed in (a) or in contact with (b) MilliQ water, 0.9% wt NaCl isotonic solution, and fetal bovine serum (FBS).

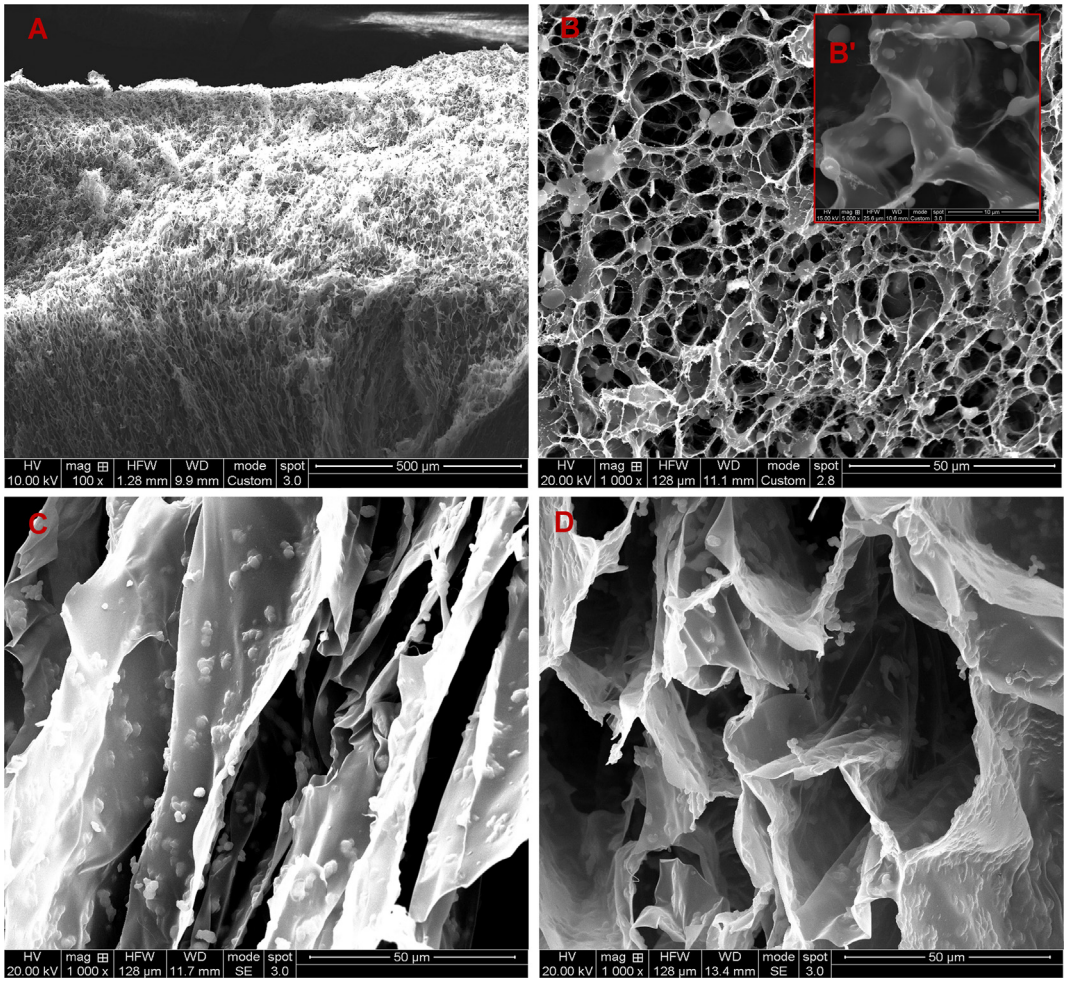

Fig. 2. SEM micrographs of the as-prepared film (A-B, B′) and films incubated for 24 h in water (C, D).

wound care [15,16]. Continuous or semi-continuous interrogations and readouts can reduce the frequency of medical interventions by signalling conditions that require attention, and enable data collection to resolve predictive trends and elaborate more efficacious therapies [16,17].

While technologies that detect specific markers of the wound healing process still need to await a clearer understanding of the chronic wound biochemistry, hydration and temperature are two parameters already identified to be critical for healing [18].

Early detection of bacterial infection is a valuable information to avoid complications. Likewise, indication of absence of infection is also important to avoid unnecessary inspections and dressing changes, and overuse of antibiotics with the connected risk of development of antibiotic-resistant strains [4]. One early indication of bacterial infection is heat production. Therefore, an accurate measurement of temperature can be used to create an alert for a potential infectious state [19].

Ideally, the sensors used for the application should be almost invisible and fully integrated in the dressing [15]. We have already proposed the concept of coupling hydrogel films with inexpensive, lightweight, UHF RFID sensor tags to produce hydrogel wound dressings that can battery-less monitor temperature and moisture level of the bandage in contact with the skin [20], as well as wireless transmit

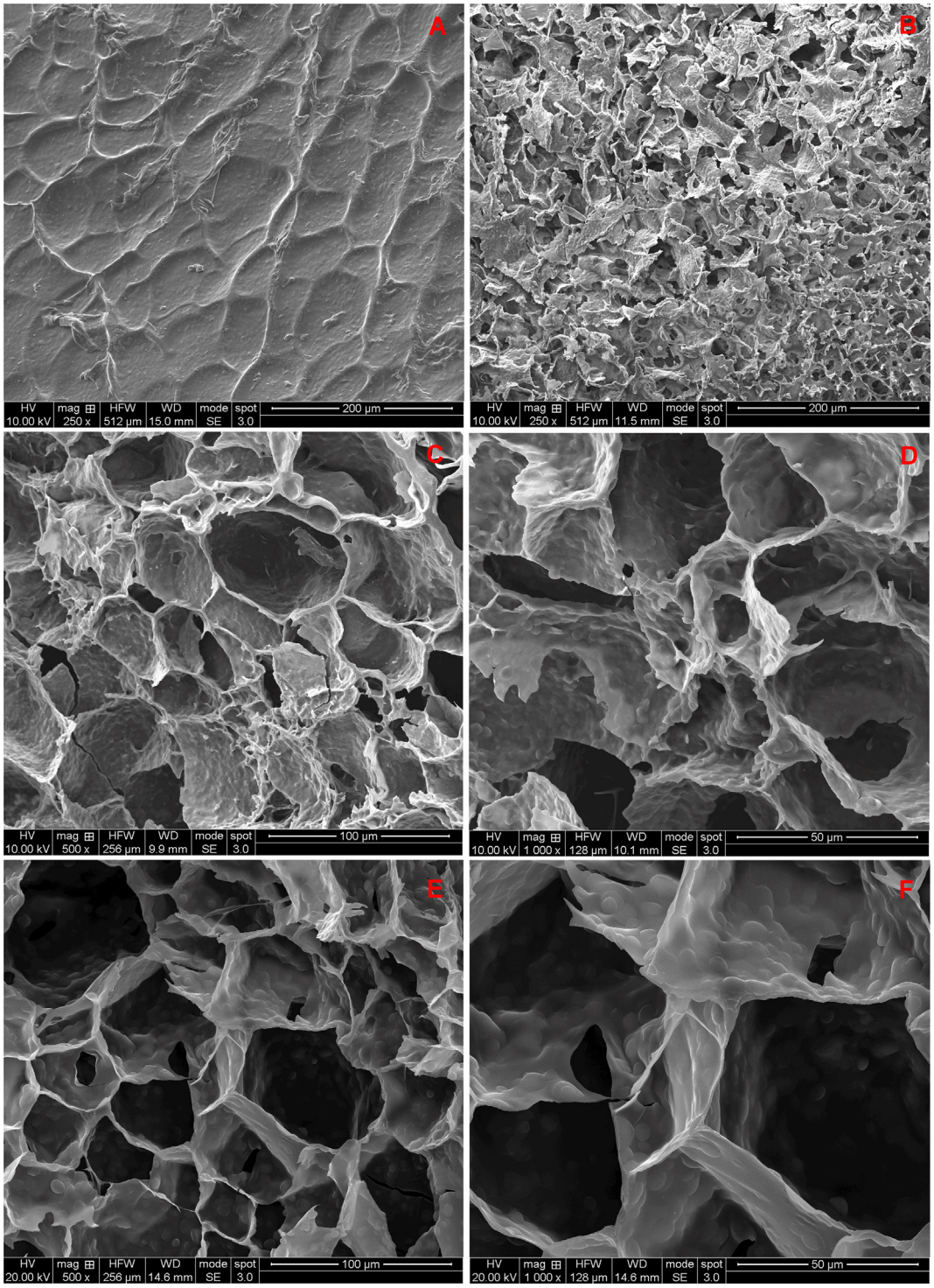

Fig. 3. SEM micrographs of the surfaces of films after immersion for 6 h in FBS, before (A) and after (B) rinsing with water; cross-section of the above film at two magnifications (C, D); cross-section of the film after immersion in saline solution for 24 h at two magnifications (E, F).

the measured data to an off-body reader. The rationale of the proposed dressing resides in the possibility of using the hydrogel membrane contemporarily as a medical device, a sensor and a substrate for electronics and communication platform. A *self-sensing* passive device is therefore obtained, wherein *the antenna is also the sensor* [21–23].

For this purpose, hydrogel formulations based on a blend of xyloglucan (XG) and polyvinyl alcohol (PVA), chemically crosslinked with glutaraldehyde (GA) have been developed [24]. Xyloglucan is an interesting polysaccharide, abundant and relatively inexpensive. It is reported to have intrinsic anti-inflammatory properties and synergistic effects with other anti-inflammatory agents when used for topical administration to the skin or to the buccal mucosa [25]. In wound healing, tamarind seed XG extracts, with ca. 65% of xyloglucan, have been demonstrated to be able to improve re-epithelialization and remodeling processes [26,27].

The aim of the present study is to investigate the XG-PVA hydrogel swelling behavior in simulated biological fluids, such as isotonic saline solution and fetal bovine serum, and the induced changes in hydrogel

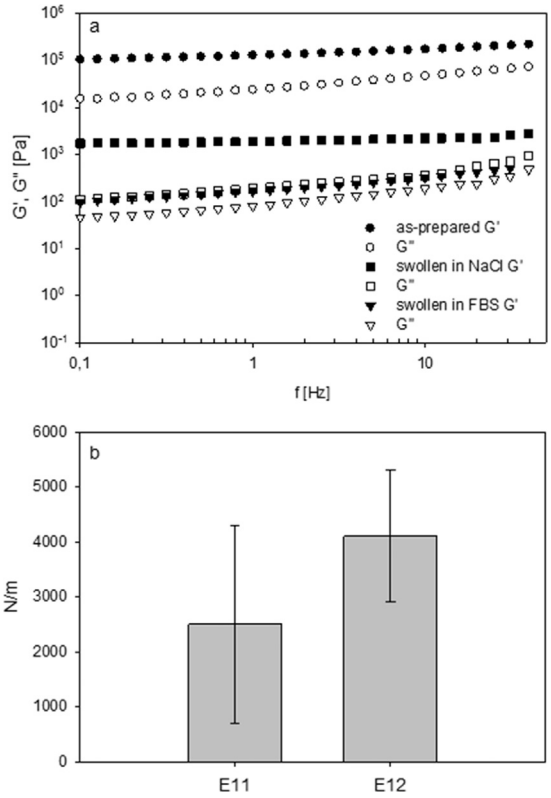

Fig. 4. Dynamic mechanical spectra of as-prepared, saline solution- and FBS-swollen films (a); membrane elastic moduli (b).

morphology, mechanical and dielectric properties. In particular, the dielectric characterization has been performed in two wide frequency regions; 10^0–10^6 Hz and 10^8–10^{11} Hz. Indeed, the modifications of the dielectric properties of the film caused by the absorbed fluids affect the response of the integrated RFID tag antenna, being the basis of the proposed sensing mechanism. Hence, the hydration level of both dressing and wound can be retrieved from the analysis of the variation of the communication parameters between tag and off-body reader.

2. Materials and methods

2.1. Preparation of XG-PVA hydrogel films

Tamarind xyloglucan (XG) was kindly provided by DSP Gokyo Food and Chemical Co. (Japan) with a molar ratio among glucose, xylose and galactose units of 2.8:2.25:1 [28,29]. XG molecular weight was measured by static light scattering, via Zimm plot analysis, and resulted 1.185 ± 0.085 MDa [24]. Poly(vinyl alcohol) (PVA, MW = 16 kDa, 98% degree of deacetylation) was purchased from Sigma-Aldrich. The two polymers were individually dissolved in water by overnight stirring (4% w/v XG at room temperature, 2% w/v PVA at 80 °C). The solutions were mixed at 1:1 vol ratio for 30 min, acidified to pH 2.5 (1 M HCl), and added with glutaraldehyde (GA, Sigma Aldrich). Stirring was continued for 1 h at room temperature, then NaOH (1 M) was added to increase pH to 7.0. Finally, glycerol (Gro, Sigma Aldrich) was added. The solution was casted into glass moulds and incubated in an environmental chamber at room temperature and 50% relative humidity (RH) to a constant weight.

Films were washed with a mixture of MilliQ water/Gro and air-dried at 50% RH. Films of different thickness were obtained by casting different volumes of solution. The thickness, reported as average value of ten measurements per approx. 12 cm^2, was measured with a Baxlo 4000 instrument.

The insoluble fraction (GF, %) and the residual water content (RWC, %) were measured for each preparation batch, as described in detail in Ref. [24]. In particular, GF = 93 ± 3% and RWC = 15 ± 2% were determined. The films will be named hereafter “as-prepared”.

2.2. Swelling tests

Swelling tests were carried out with two set-ups, upon direct immersion of samples in the swelling medium, and by placing them on 6-well plates equipped with transwell inserts. The as-prepared samples were exposed to the medium for determined periods of time, then removed from the solvent, blotted with filter paper and weighed. Temperature was kept at 25 °C.

The swelling degree was calculated using the following equation:

$$SD\% = (W_s - W_d)/W_d \times 100$$

where W_s corresponds to the hydrated weight of the sample and W_d represents the weight of the as-prepared sample. MilliQ water, 0.9% wt NaCl and fetal bovine serum (FBS) were used as swelling media.

2.3. Scanning electron microscopy (SEM)

Surface morphology was imaged by a Field Emission Scanning Electron Microscope (FESEM-JEOL) at an accelerating voltage of 10 kV. Unless otherwise stated, films were rinsed with water for 30 min before freeze-drying. Freeze-dried samples were fractured in liquid nitrogen to expose also their inner structure, mounted on SEM aluminium stubs by means of a graphite adhesive layer and coated with a gold layer by JFC-1300 gold coater (JEOL) for 90 s at 30 mA before scanning.

2.4. Rheological measurements

Rheological measurements were performed on a stress-controlled AR-G2 rheometer (TA Instruments, USA) using a plate/plate geometry with the gap ranging from 70 to 100 and 800 to 1000 μm for as-prepared and swollen films, respectively. Viscoelastic spectra were done in the frequency range 0.1–80 Hz with a strain of 0.01, well within the linear viscoelastic region. The films were gently placed on the rheometer plate, set at the temperature of 20 °C. All measurements were done in triplicate.

2.5. Biaxial tension measurements

Biaxial tension tests were performed with a Bose® planar biaxial TestBench instrument equipped with four 250 N electromagnetic engines. From the water swollen hydrogel films, 20 × 20 × 0.6 mm specimens were obtained by means of a regular cutter and fixed to four clamps, each corresponding to one motor. The tests were carried out in displacement control by stretching the specimen in each direction, at a speed of 1 mm/s. The forces in two directions were monitored by means of two 250 N load cells. The strains field at the specimen surface were obtained with a digital video extensometer (DVE) assuming as reference length the position of five markers (four at the corners and one at the center). Displacements were monitored by a 1024 × 468 pixel digital camera with a refresh rate of 50 Hz. The measurement set up is shown in Fig. S1 of Supplementary information. Results obtained were averaged on 5 measurements carried out on different samples.

2.6. Electrochemical impedance spectroscopy (EIS)

Solartron FRA (Frequency Response Analyzer)-12558 instrument with a Dielectric Interface-1249, connected to a cell with two gold-coated, 2.1 cm diameter electrodes, was used to measure the electrochemical impedance of hydrogel films at room temperature, in the frequency range 10^0 and 10^6 Hz, under 0.2 V bias. Measurements were carried out on the as-prepared films and upon addition of known amounts of isotonic 0.9% wt NaCl solution. Data were represented in

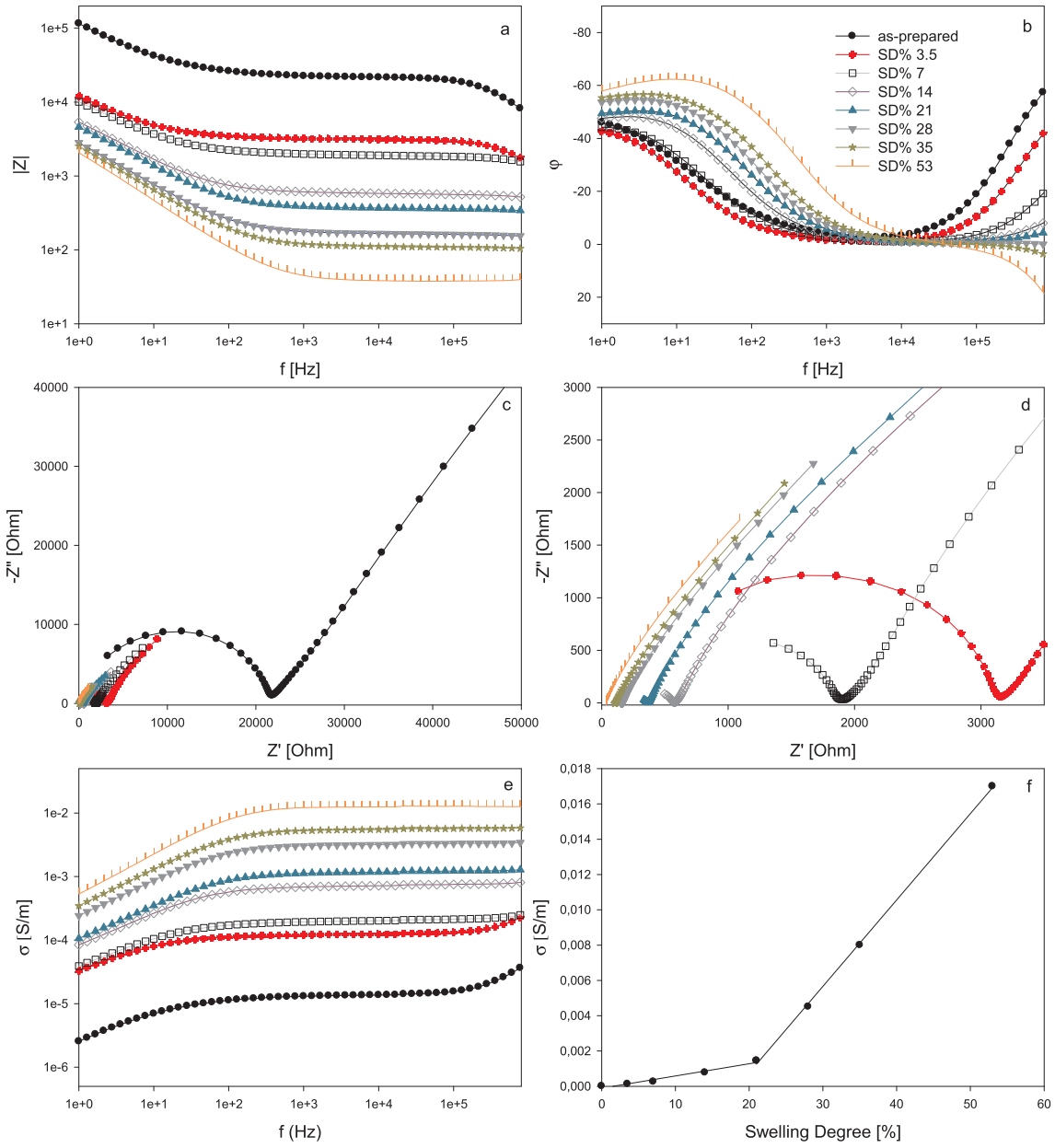

Fig. 5. Electrical impedance spectroscopy of the hydrogel films as function of the swelling degree. Bøde (a, b) and Nyquist (c, d) diagrams; conductivity as function of frequency (e); and conductivity values at f = 1 kHz as function of the swelling degree (f).

terms of Bode (impedance modulus and phase angle as function of frequency) and Nyquist (imaginary and real components of complex impedance) diagrams. Furthermore, we adopted the formalisms of complex impedance, Z^*, and permittivity, ε^*, to determine the bulk conductivity, σ, of the films [30–32]. According to this approach, the complex dielectric function can be calculated as:

$$\varepsilon^*(\omega) = \frac{Y^*}{i\omega C_0} = \frac{C}{C_0} - i\frac{G}{\omega C_0} = \varepsilon'(\omega) - \varepsilon''(\omega)$$

where $Y^* = [Z^*(\omega)] - 1$ is the measured complex admittance, C and G are the measured capacitance and conductance, ω the angular frequency ($\omega = 2\pi f$) and C_0 the equivalent capacitance of the free space.

The frequency-dependent AC conductivity, σ′(ω), is then obtained as [31]:

$$\sigma'(\omega) = \varepsilon''(\omega)\omega\varepsilon_0$$

where ε_0 is the permittivity of free space and ε″ the imaginary part of complex permittivity.

2.7. Radiofrequency (RF) characterization

The dielectric-properties, permittivity and conductivity (ε_r,σ),of the hydrogel films were evaluated in the 200–1500 MHz region by using a modified multilayer microstrip ring resonator [33]. The measurement system, shown in Fig. S2 of Supplementary Information, is composed by the ring and the ground plane/feed network, located in separate planes [34] to enable the easy placement of the sample between the two layers. Compared to conventional single-layer resonators, the multilayer structure enables also a stronger interaction between the sample and the ring fields, forcing the latter to physically cross the sample before coupling with the ground plane. This feature is particularly important for thin film characterization such as the hydrogel films here evaluated.

In the case under test, the dielectric properties of the hydrogel film were estimated through a combined experimental and numerical procedure. Measurements of the transmission scattering parameter S_{12} (i.e. the ratio between the RF signal coming out of the port 1 of the ring

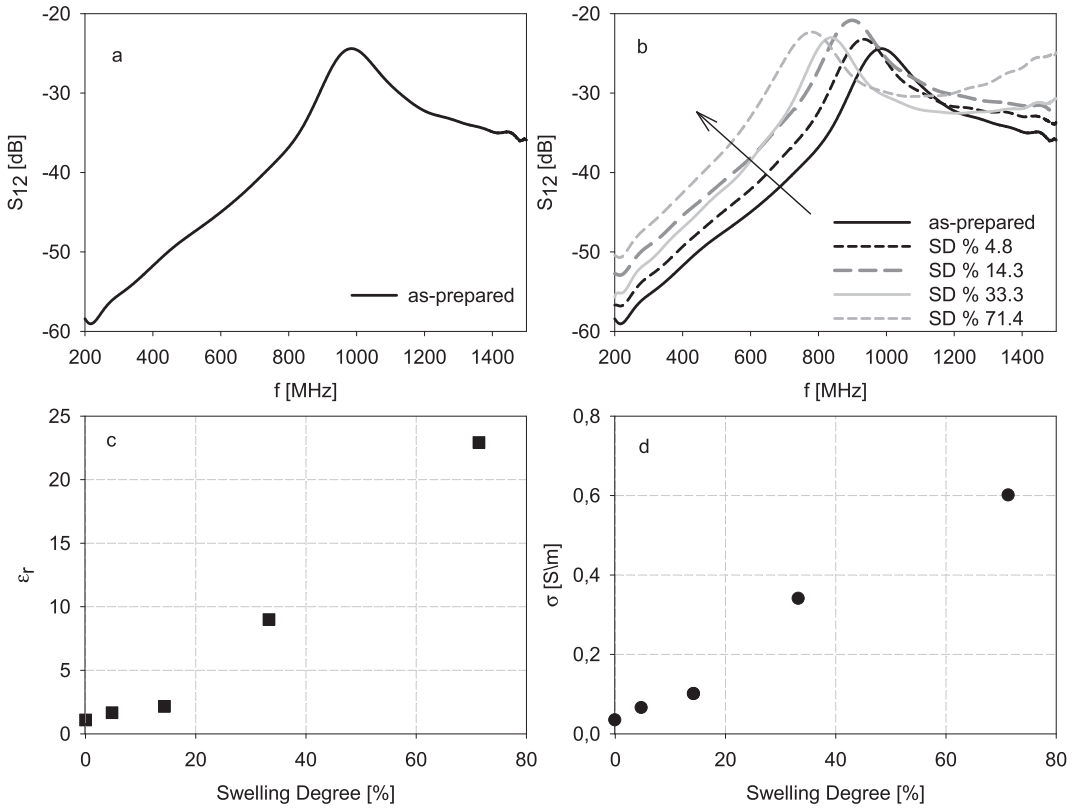

Fig. 6. Measured transmission scattering parameters S_{12} for the as-prepared film (a); S_{12} measurements vs frequency during the progressive absorption of saline solution (b); estimated dielectric permittivity (c) and electric conductivity (d) of the hydrogel films vs. swelling degree (%).

when a signal is injected inside port 2) versus frequency were carried out by using a Vector Network Analyzer.

In parallel, a numerical model of the multilayer ring resonator, including the sample, is computed by a Finite Element Method (FEKO implementation, https://www.feko.info). The peak frequency, f_R, and the quality factor, Q, defined as:

$$Q = f_R / |f_{max} - f_{min}|_{-3dB}$$

of the measured/simulated S_{12} parameter, intrinsically brings information about the unknown permittivity and conductivity of the sample.

An identification procedure of the electromagnetic parameters of the film is hence performed by varying in simulation the trial permittivity and conductivity of the sample in a suitable range and by computing the corresponding numerical features. The optimal identification of the electromagnetic parameters of the film is then achieved by minimizing the error between simulated and measured data.

The XG-PVA hydrogel sample under test (thickness 0.17 mm, diameter 8.5 cm, initial weight 2.1 g) was characterized as-prepared as well as during the progressive absorption of 0.9% wt NaCl solution. The dynamic exposure of the film to body fluid was simulated by placing the film on a synthetic sponge soaked with saline solution (ε_r = 75.2, σ = 1.67 S/m at 870 MHz) for a fixed time interval (2 min); then, the film was placed between the two layers of the ring resonator and the S_{12} scattering parameter versus frequency was measured. A digital scale was used to monitor the fluid uptake by continuously weighing the film after each exposure to the fluid.

3. Results and discussion

3.1. Swelling of XG-PVA films by simulated biological fluids

Chemically crosslinked hydrogels were prepared from solutions of XG and PVA by addition of glutaraldehyde. The preparation and chemical structure of these films has been described in detail in a previous work [24]. In particular, the formulation selected for the present study is a covalent network obtained through the formation of glutaraldehyde-mediated crosslinks between the polymeric components of the formulation (XG-XG, XG-PVA and PVA-PVA). Covalent crosslinks increase the crosslinking density and solvent-resistance of these systems with respect to their physical networks, where the crosslinking points are mainly represented by associated domains of xyloglucan chains [24]. Besides, glycerol that is added to the formulation prior to casting and air-drying is also partially grafted to the network, increasing the network mesh size and providing high flexibility to the films.

In Fig. 1a-b, the swelling curves of the samples exposed to water, saline solution, and serum are shown. It is important to note that when the films are exposed to any of the above media, they can uptake the various components of the swelling media, primarily water, and concurrently release glycerol and other hydrogel components that are not covalently attached to the network. Films immersed in pure water initially swell fast, attaining the 80% of their equilibrium swelling value in 10 min, and reach a plateau in ca. 8 h. Films in their equilibrium swollen state maintain their initial shape and elasticity. The presence of sodium chloride in the saline solution reduces both swelling rate and swelling degree at plateau, since salt decreases the chemical potential of water in the swelling medium and, in turn, the osmotic contribution to the swelling pressure.

Samples immersed in FBS change their consistency becoming swollen and slimy, thus difficult to handle. For this reason, the measurements in FBS with this set-up were interrupted after 6 h. This behavior suggests that the films absorb components of the serum that change their consistency. The swelling measurements in water and saline solution were continued beyond the attainment of the equilibrium conditions for further 18 h in order to probe the films integrity when immersed in these media for longer times. We do not observe any

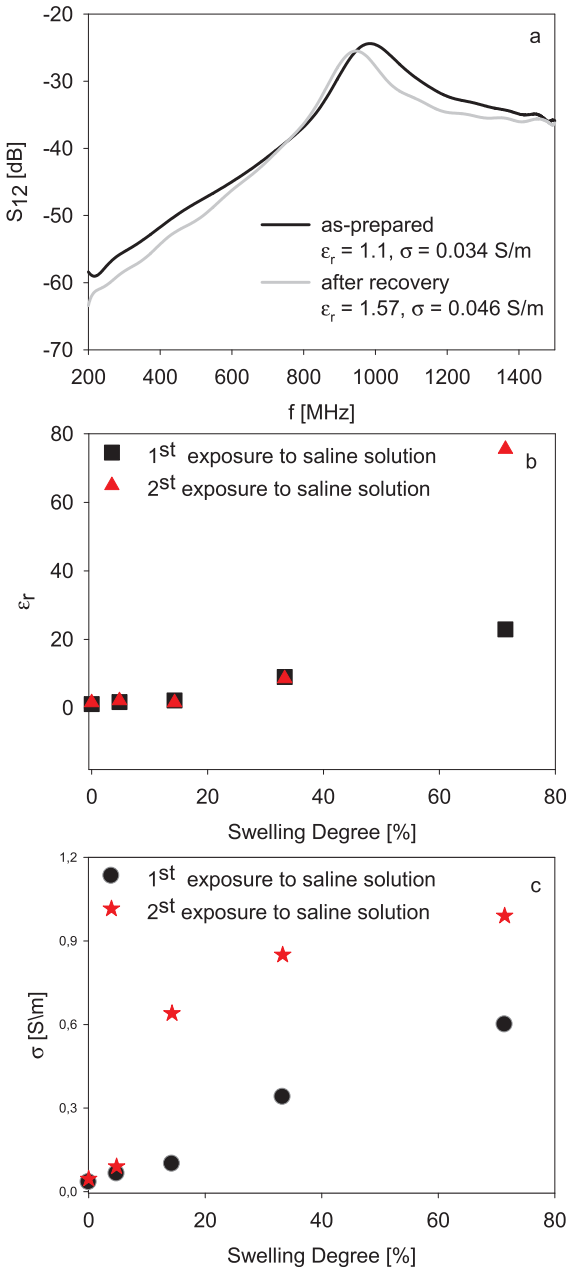

Fig. 7. Measured transmission scattered parameter S_{12} in as-prepared state and after swelling and "recovery" of the initial weight (a); Overlapped estimated dielectric properties of the sample vs. % swelling degree of the membrane in the case of two consecutive exposures to the saline solution (b, c).

significant change of weight or shape of the films.

When films were exposed to the various swelling media through a porous membrane (Fig. 1b), set-up that better simulates the solvent exchange conditions of wound dressings, they swelled more slowly. The SD% at plateau for water was similar to the value measured upon immersion, while the SD% obtained for isotonic saline solution and FBS resulted slightly lower, due to the formation of a thin and relatively dry skin on the surface that is exposed to air. Also, we observe a difference in the behavior of the films swollen with serum with respect to those swollen by the other two media when the experiments are carried out with the two different set-ups. In facts, hydrogels immersed in FBS, then blotted and weighed, show a similar weight increase to water. Conversely, when they are in contact with FBS through the porous membrane of the transwell support, their behavior resembles the one in saline solution. We can argue that the solutes present in FBS contribute to occlude some of the film pores, as it will be further discussed in the next paragraph. This problem is reflected also in the higher error bars for these measurements, which also suffer for the difficulty in removing all fluid present inside and above the porous membrane.

3.2. Microstructure of as-prepared and equilibrium swollen films

In Fig. 2, SEM micrographs of as-prepared (Fig. 2A-B, B′) and water-swollen (Fig. 2C-D) films for 24 h are shown. In particular, Fig. 2a shows both surface and cross-section of the as-prepared film. The surface of the film is characterised by adjoined irregular tubular structures, while the cross-section (also shown in Fig. 2B and its inset, 2B′) shows uniformly distributed pores, yet heterogeneous in size. Small globules, probably caused by highly crosslinked regions, are randomly distributed on the pore walls. The tubular structure resembles the one observed in hydrogels of partially degalactosylated xyloglucans (Deg-XG), produced by temperature-induced gelation, where orthogonally stacked lamellae interconnected by thin walls are formed by Deg-XG chains self-assembly [35]. Here, the higher degree of branching of the native (non degalactosylated) XG, together with the presence of glycerol and PVA in the formulation, reduces the ability of XG chains to align into foils and leads to hydrogels with less regular microstructure and higher degree of porosity.

After immersion in water for 24 h, hydrogels attain their equilibrium swelling state and show a significant change in their microstructure. The lamellae are characterised by thicker walls and higher spacing (see Fig. 2C), the pore size becomes larger and globules appear more densely distributed (see Fig. 2D). This more open microstructure is in good agreement with the observed increase of swelling degree.

In Fig. 3(A-B), SEM micrographs of the sample surface that was kept immersed in FBS for 6 h, before (Fig. 3A) and after (Fig. 3B) rising with water, are reported. It is evident that serum components strongly adsorb on the film surface, creating a compact layer that fills the pores. This explains the observed dramatic change in film consistency. Even after thorough rinsing with water, the pores are still partially occluded. This is evident from the observation of both surface and cross-section of the samples (Fig. 3C, D). The FBS-swollen and the saline-solution swollen systems (see Fig. 3E, F) have similar average pore-size. The relatively high swelling degree of samples immersed in FBS with respect to those immersed in saline solution can be possibly attributed to the protein serum uptake.

3.3. Mechanical properties

The rheological behavior of the swollen XG-PVA films was investigated by dynamic mechanical analysis. Films were swollen with the two simulated biological fluids, saline solution or FBS, up to their maximum absorbance capacity (ca. 6 h). Storage shear modulus, G′, and loss modulus, G″, curves for the as-prepared and swollen films are shown in Fig. 4a. All systems show G′ curves higher than the G″ curves, and invariant or slightly increasing with frequency. Both G′ and G″ decrease for the swollen systems with respect to as-prepared films. In particular, G′ and G″ decrease of two orders of magnitude as a result of the increase in incorporated saline solution from 15% to ca. 78%. With FBS, although the incorporated amount of swelling medium is not significantly changed (ca. 79%), G′ is further decreased of one order of magnitude, whereas the reduction in G″ is less pronounced. The serum proteins may affect the inter-chain xyloglucan hydrophobic interactions, thus reducing the crosslinking density [36]. The more viscous nature of the swelling medium with respect to saline solution explains the relatively high G″ curve.

The mechanical properties of the films were also investigated by biaxial tension tests. From the stress-strain curves (here not shown), a transversely isotropic mechanical behaviour is deduced. The plane of transverse isotropy is the cross-section of the specimen and, henceforth, two different elastic moduli for the two load directions used in the

mechanical tests can be identified. The membrane stress was measured to circumvent the problem of the specimen thickness that is not rigorously constant along the specimen. Fig. 4b shows the average values of the elastic moduli in the two directions with the confidence intervals obtained from the statistics of the analysis. The anisotropic mechanical behavior is in good agreement with the SEM morphology of the freeze-dried samples, as shown in Fig. 2.

3.4. Electrical impedance properties

Electrical impedance spectroscopy was applied to measure the electric properties of the films in the as-prepared condition and at different swelling states using saline solution. In Fig. 5a-f, Bøde and Nyquist diagrams, conductivity vs. frequency plots and conductivity at 1 kHz vs. swelling degree plot are reported.

In the Bøde plots (see Fig. 5a-b) four distinct regions can be identified. For all swelling degrees, at the highest frequencies (near 1 MHz), the phase angle is strongly affected by the swelling degree; for the as-prepared film and the lower swelling degrees, the hydrogel shows capacitive-dominated behavior (negative phase angles); increasing the electrolyte content in the hydrogel, the phase angle approaches zero, indicating a prevailing resistive behavior; for the highest swelling degree, the positive phase angle suggests inductive properties. Moving in the direction of lower frequencies, a resistive behavior is always shown where the phase shift passes through ca. 0° and the impedance curve is a horizontal line (not frequency dependent). Indeed, in this frequency region the bulk resistance of the hydrogel/electrolyte system dominates the impedance. In the mid-low frequency range, all films develop a capacitive component of the impedance, as indicated by the negative $|Z|$ slope and the phase angle that becomes more negative. At low frequencies (the lower the higher is the swelling degree), the phase angle approaches $-45°$ and the impedance magnitude changes slope. This behavior is caused by the diffusion of ions through the finite thickness of the hydrogel.

The Nyquist diagrams are shown in Fig. 5c-d. The plot of the as-prepared film (Fig. 5c) is a semicircular arc at higher frequencies with an almost straight line at lower frequencies. It is worth recalling that the as-prepared film has a water content of ca. 15% and may also contain residual Na^+ and Cl^- ions from the synthesis, which can explain the observed ionic conductivity at low frequency. By increasing the swelling degree, the capacitive behavior of the hydrogel is progressively shifted to higher frequencies and the semicircles are no longer visible in the Nyquist plots.

Fig. 5e shows σ′(ω) vs. frequency plots for film swollen to different degrees. The plateau at intermediate to high frequencies (10^3–10^5 Hz) corresponds to the DC conductivity, σ_{dc}, of the films due to ions mobility. In Fig. 5f, σ′(1kHz) is plotted as a function of the swelling degree. We observe a linear dependence of conductivity with a change of slope for SD% > 20. This behavior reflects the combined effects of increased ions content and ions mobility due to the higher water content and larger porosity.

Electric impedance measurements performed on swollen films by immersion in either bidistilled water or saline-solution to the same SD % = 200 (curves not shown) show differences in conductivity for two conditions. In particular, the σ′(1 kHz) values are $6.3 \cdot 10^{-3}$ S/m and $3.7 \cdot 10^{-2}$ S/m for water-swollen and saline solution-swollen films, respectively, while σ′(1 kHz) of the as-prepared film is $7.8 \cdot 10^{-6}$ S/m. The σ′ (1 kHz) value of the water-swollen film is three order of magnitude higher than the value of the as-prepared film, this increase being essentially attributable to the higher mobility of the ions already present from the synthesis. The conductivity further increases of one order of magnitude in the saline solution-swollen system due to higher salts content.

3.5. RF characterization

The measured S_{12} scattering parameter for the as-prepared film is shown in Fig. 6a. At room temperature and humidity, the estimated permittivity of the film, ε_r, (see Fig. 6c, SD% = 0) is rather low, equal to 1.1, while conductivity (see Fig. 6d, SD% = 0) is non-negligible ($\sigma = 3.2 \times 10^{-2}$ S/m) and mainly related to the presence of residual water and ions from the fabrication. The radiofrequency response of the hydrogel film significantly changes along with the amount of absorbed saline solution. The increase of permittivity and electric conductivity of the hydrogel produces a progressive frequency shift of the S_{12} curves (Fig. 6b) that spans in the frequency range $780 < f < 985$ MHz that are correlated to a monotonic change of the dielectric properties of the hydrogel film (Fig. 6c-d) as a function of SD%. In the selected frequency band, the film exhibits variations of permittivity and electrical conductivity of about one order of magnitude, with a change of slope for SD % > 20 similar to the one observed in the lower frequency range.

In order to verify the “recovery” capability of the system, the film was left to air-dry at room temperature and humidity. Then, its weight was monitored every hour, until the film attained its initial weight. A comparison between the measured S_{12} in the case of the as-prepared film and the S_{12} measured after the recovery process is shown in Fig. 7a. Despite the slight frequency shift, that can be caused by the change of film composition after its swelling with the saline solution and air-drying that causes absorbed salts precipitation, the dielectric properties of the film are comparable.

Finally, with the purpose of assessing the reproducibility of the electromagnetic features versus multiple swelling cycles, the same film was again exposed to the saline solution by repeating the measurement procedure described above. The overlapped results related to the estimated dielectric properties as a function of the swelling degree are shown in Fig. 7b-c. The agreement between data is particularly good in the early stages of the phenomena, i.e. for low values of ε_r and σ. Discrepancies are instead visible for the higher degree of swelling, probably due to the irreversible modifications of the film during the first exposure cycle, comprising loss of glycerol, microstructure rearrangement and increase of salt concentration.

4. Concluding remarks

Research which addresses advanced wound management can contribute to the needs of modern healthcare, especially in situations that require continuous monitoring, analysis, responsive therapeutic treatments and data recording. The development of ‘smart’ bandages and dressings that can remotely monitor relevant parameters for the wound healing process without a hospital intervention can be very useful tools for patients and physicians and for advancing the understanding of the healing process. We developed a hydrogel dressing suitable to integrate sensing and communication platforms for remote monitoring.

In particular, we demonstrated that an increase of swelling degree up to 60%, still much lower than the equilibrium swelling value (280% in saline solution) affects the conductivity of the film up to 10^3 times in the kHz frequency region and 10 times in the UHF range, confirming that these films can be further exploited for sensing applications, according to the well-known *sensor-less approach*. Most of this conductivity increase is due to the increase of mobility of residual sodium and chlorine ions from the synthesis. This observation suggests the possibility of pre-loading the hydrogel with small amounts of ions with various charge densities and mobilities to modulate the impact of water uptake on the electromagnetic properties of the film, and in turn the response of the RFID antenna.

A parallel biological study on the same hydrogels films is demonstrating that they are non-cytotoxic, fully hemocompatible, non-adhesive to the wound and able to provide protection from bacterial infiltration [37]. These results altogether encourage in proceeding with further development and evaluation of these hydrogel membranes as

smart wound dressings.

Data availability

The raw/processed data required to reproduce these findings cannot be shared at this time due to technical or time limitations.

Acknowledgments

We gratefully acknowledge DSP Gokyo, Food and Chemical Co., Japan, and particularly Dr. K. Yamatoya, Dr. M. Shirakawa, Dr. A. Tabuchi for supplying the xyloglucan sample.

Appendix A. Supplementary material

Supplementary data associated with this article can be found, in the online version, at https://doi.org/10.1016/j.eurpolymj.2018.07.038.

References

[1] K. Järbrink, G. Ni, H. Sönnergren, A. Schmidtchen, C. Pang, R. Bajpai, J. Car, The humanistic and economic burden of chronic wounds : a protocol for a systematic review, Syst. Rev. 6 (2017) 1–7, https://doi.org/10.1186/s13643-016-0400-8.
[2] M. Turns, The diabetic foot: an overview of assessment and complications, Br. J. Nurs. 20 (2011) S19–S25, https://doi.org/10.12968/bjon.2011.20.Sup8.S19.
[3] R.G. Frykberg, J. Banks, Challenges in the treatment of chronic wounds, Adv. Wound Care 4 (9) (2015) 560–582, https://doi.org/10.1089/wound.2015.0635.
[4] A.R. Siddiqui, J.M. Bernstein, Chronic wound infection: Facts and controversies, Clin. Dermatol. 28 (2010) 519–526, https://doi.org/10.1016/j.clindermatol.2010.03.009.
[5] G.D. Winter, Formation of the scab and the rate of epithelization of superficial wounds in the skin of the young domestic pig, Nature 193 (1962) 293–294, https://doi.org/10.1038/193293a0.
[6] L.G. Ovington, Advances in wound dressings, Clin. Dermatol. 25 (2007) 33–38, https://doi.org/10.1016/j.clindermatol.2006.09.003.
[7] J.S. Boateng, K.H. Mattews, H.N.E. Stevens, G.M. Eccleston, Wound healing dressings and drug delivery systems: a review, J. Pharm. Sci. 97 (8) (2008) 2892–2923, https://doi.org/10.1002/jps.21210.
[8] K. Deligkaris, T.S. Tadele, W. Olthuis, A. van den Berg, Hydrogel-based devices for biomedical applications, Sensors Actuat. B Chem. 147 (2010) 765–774, https://doi.org/10.1016/j.snb.2010.03.083.
[9] N.A. Peppas, Y. Huang, M. Torres-Lugo, J.H. Ward, J. Zhang, Physicochemical foundations and structural design of hydrogels in medicine and biology, Annu. Rev. Biomed. Eng. 9–29 (2000).
[10] N.A. Peppas, J.Z. Hilt, A. Khademhosseini, R. Langer, Hydrogels in biology and medicine: From molecular principles to bionanotechnology, Adv. Mater. 18 (2006) 1345–1360, https://doi.org/10.1002/adma.200501612.
[11] J.C. Dumville, S. O'Meara, S. Deshpande, K. Speak, Hydrogel dressings for healing diabetic foot ulcers, Cochrane Database Syst. Rev. 9 (2011) 1–46, https://doi.org/10.1002/14651858.CD009101.pub2.
[12] S. Dhivya, V. Vijaya, E. Santhini, Wound dressings – a review, BioMedicine. 5 (2015) 24–28, https://doi.org/10.7603/s40681-015-0022-9.
[13] K. Ousey, K.F. Cutting, A.A. Rogers, M.G. Rippon, The importance of hydration in wound healing: reinvigorating the clinical perspective, J. Wound Care. 25 (2016) 122–130, https://doi.org/10.1520/D0850-11.1.
[14] K.-T. Huang, Y.-L. Fang, P.-S. Hsieh, C.-C. Li, N.-T. Dai, C.-J. Huang, Zwitterionic nanocomposite hydrogels as effective wound dressings, J. Mater. Chem. B 4 (2016) 4206–4215, https://doi.org/10.1039/C6TB00302H.
[15] V. Rawal, A. Dhamija, S. Gupta, Recent advancements in wearable bio-sensor applications, Int. J. Sci. Res. Eng. Technol. 1 (2012) 154–159.
[16] T.R. Dargaville, B.L. Farrugia, J.A. Broadbent, S. Pace, Z. Upton, N.H. Voelcker, Sensors and imaging for wound healing: A review, Biosens. Bioelectron. 41 (2013) 30–42, https://doi.org/10.1016/j.bios.2012.09.029.
[17] S.D. Milne, I. Seoudi, H. Al Hamad, T.K. Talal, A.A. Anoop, N. Allahverdi, Z. Zakaria, R. Menzies, P. Connolly, A wearable wound moisture sensor as an indicator for wound dressing change: An observational study of wound moisture and status, Int. Wound J. (2015) 1–6, https://doi.org/10.1111/iwj.12521.
[18] N. Mehmood, A. Hariz, R. Fitridge, N.H. Voelcker, Applications of modern sensors and wireless technology in effective wound management, J. Biomed. Mater. Res. - Part B Appl. Biomater. 102 (2014) 885–895, https://doi.org/10.1002/jbm.b.33063.
[19] G. Nakagami, H. Sanada, S. Iizaka, T. Kadono, T. Higashino, H. Koyanagi, N. Haga, Predicting delayed pressure ulcer healing using thermography: a prospective cohort study, J. Wound Care. 19 (2010) 465–472, https://doi.org/10.12968/jowc.2010.19.11.79695.
[20] C. Occhiuzzi, A. Ajovalasit, M.A. Sabatino, C. Dispenza, G. Marrocco, RFID epidermal sensor including hydrogel membranes for wound monitoring and healing, in: 2015 IEEE Int. Conf. RFID, RFID 2015, 2015. http://doi.org/10.1109/RFID.2015.7113090.
[21] C. Occhiuzzi, S. Caizzone, G. Marrocco, Passive UHF RFID antennas for sensing applications: Principles, methods, and classifications, IEEE Antennas Propagat. Mag. 55 (2013) 14–34.
[22] S. Amendola, G. Bovesecchi, P. Coppa, G. Marrocco, Thermal characterization of epidermal RFID sensor for skin temperature measurements, in: 2016 IEEE Antennas Propag. Soc. Int. Symp. APSURSI 2016 – Proc, 2016, pp. 461–462. http://doi.org/10.1109/APS.2016.7695939.
[23] S. Amendola, G. Marrocco, Optimal performance of epidermal antennas for UHF radio frequency identification and sensing, IEEE Trans. Antennas Propag. 65 (2017) 473–481, https://doi.org/10.1109/TAP.2016.2639829.
[24] A. Ajovalasit, M.A. Sabatino, S. Todaro, S. Alessi, D. Giacomazza, P. Picone, M. Di Carlo, C. Dispenza, Xyloglucan-based hydrogel films for wound dressing: structure-property relationships, Carbohydr. Polym. 179 (2018) 262–272, https://doi.org/10.1016/j.carbpol.2017.09.092.
[25] I. Giori, A. Arpini, S. Togni, Tamarind seed polysaccharide for use in the treatment of inflammatory diseases, WO2011147768 A1, 2011.
[26] M. Yusof bin Mohamad, H.B. Akram, D. Najwa Bero, M. Tariqur Rahman, Tamarind seed extract enhances epidermal wound healing, Int. J. Biol. 4 (2012) 81–88, https://doi.org/10.5539/ijb.v4n1p81.
[27] W. Nie, A.M. Deters, Tamarind seed xyloglucans promote proliferation and migration of human skin cells through internalization via stimulation of proproliferative signal transduction pathways, Dermatol. Res. Pract. 2013 (2013) 1–14, https://doi.org/10.1155/2013/359756.
[28] P. Lang, G. Masci, M. Dentini, V. Crescenzi, D. Cooke, J. Gidley, C. Fanutti, J.S.G. Reid, Tamarind seed polysaccharide : preparation, characterisation and solution properties of carboxylated, sulphated and alkylaminated derivatives, Carbohydr. Polym. 17 (1992) 185–198, https://doi.org/10.1016/0144-8617(92)90003-9.
[29] A.D. Kulkarni, A.A. Joshi, C.L. Patil, P.D. Amale, H.M. Patel, S.J. Surana, V.S. Belgamwar, K.S. Chaudhari, C.V. Pardeshi, Xyloglucan: A functional biomacromolecule for drug delivery applications, Int. J. Biol. Macromol. 104 (2017) 799–812, https://doi.org/10.1016/j.ijbiomac.2017.06.088.
[30] P. Pissis, A. Kyritsis, Electrical conductivity studies in hydrogels, Solid State Ionics. 97 (1997) 105–113, https://doi.org/10.1016/S0167-2738(97)00074-X.
[31] B. Macdonald, J. Evgenij, Ross (Eds.), Impedance Spectroscopy: Theory, Experiment, and Applications, Wiley, 2005.
[32] C. Dispenza, C. Lo Presti, C. Belfiore, G. Spadaro, S. Piazza, Electrically conductive hydrogel composites made of polyaniline nanoparticles and poly(N-vinyl-2-pyrrolidone), Polymer 47 (2006) 961–971, https://doi.org/10.1016/j.polymer.2005.12.071.
[33] S. Amendola, C. Occhiuzzi, A. Ajovalasit, M.A. Sabatino, C. Dispenza, G. Marrocco, Dielectric characterization of biocompatible hydrogels for application to Epidermal RFID devices, in: Conf. Proceedings; 2015 45th Eur. Microw. Conf. Proceedings, EuMC, 2015, pp. 379–382. http://doi.org/10.1109/EuMC.2015.7345779.
[34] I. Waldron, S.N. Makarov, S. Biederman, R. Ludwig, Suspended ring resonator for dielectric constant measurement of foams, IEEE Microw. Wirel. Components Lett. 16 (2006) 496–498, https://doi.org/10.1109/LMWC.2006.880708.
[35] S. Todaro, M.A. Sabatino, M.R. Mangione, P. Picone, M.L. Di Giacinto, D. Bulone, C. Dispenza, Temporal control of xyloglucan self-assembly into layered structures by radiation-induced degradation, Carbohydr. Polym. 152 (2016) 382–390.
[36] A. Benichou, A. Aserin, N. Garti, Protein-polysaccharide interactions for stabilization of food emulsions, J. Dispersion Sci. Technol. 23 (2002) 93–123.
[37] A. Ajovalasit, Xyloglucan-based hydrogels: a biomaterials chemistry contribution towards advanced wound dressings (Doctoral dissertation), Universita degli studi di Palermo, Italy, 2018.